Contents of Supplementary Figures

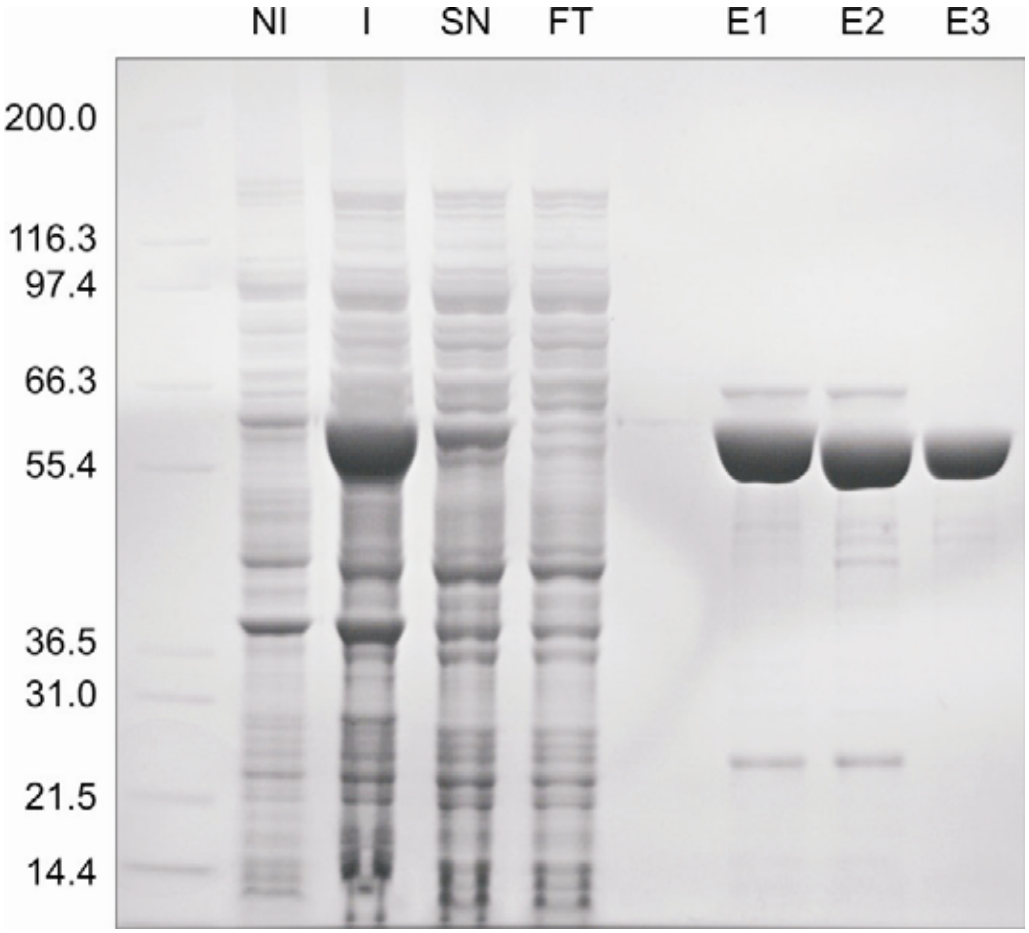

Supplementary Fig. 1: Expression and purification of mouse EHD2. Mouse EHD2 was expressed in *Escherichia coli* as a His-fusion protein as described in Materials and Methods. NI - Non-induced culture. I - Induced culture. SN - Soluble extract. FT – Soluble extract after application to NiNTA Sepharose. E1- EHD2 after elution from NiNTA-Sepharose. E2 – EHD2 after dialysis and thrombin cleavage. E3 – EHD2 after re-application and elution from the NiNTA column. This protein was further purified by size-exclusion chromatography using a Sephadex S200 column (data not shown).

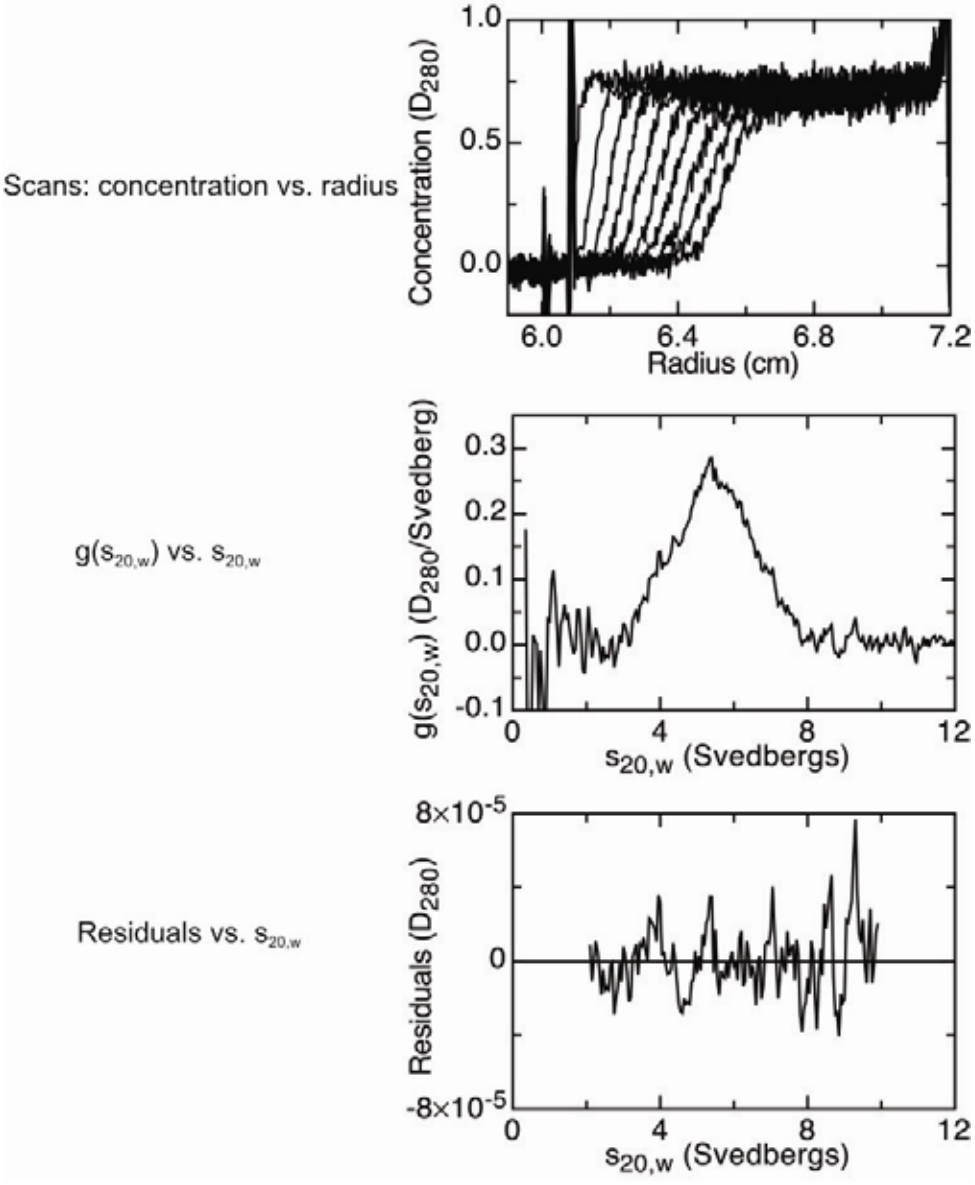

Supplementary Figure 2: Ultracentrifugation analysis indicates that EHD2 is a dimeric protein. Sedimentation velocity experiments were performed as described in methods at 300 mM NaCl. Selected scans (at equal, ~15 min intervals), and of $g(s_{20,w})$ (the amount of material sedimenting between $s_{20,w}$ and ($s_{20,w}+\delta s$)) and also the residuals for fitting the data with DCDT+, were plotted with the program profit v.5.6.7 (Quantum soft, Switzerland). The fitted value is 113 ± 4 kDa which corresponds well with the calculated mass of the dimer of 124 kDa.
We also observed an EHD2 dimer by size-exclusion chromatography and by dynamic light scattering (data not shown). At 50 μM protein concentration, the hydrodynamic radius did not change in the presence or absence of nucleotides (or in 150 mM versus 300 mM NaCl), as judged by dynamic light scattering experiments (data not shown).

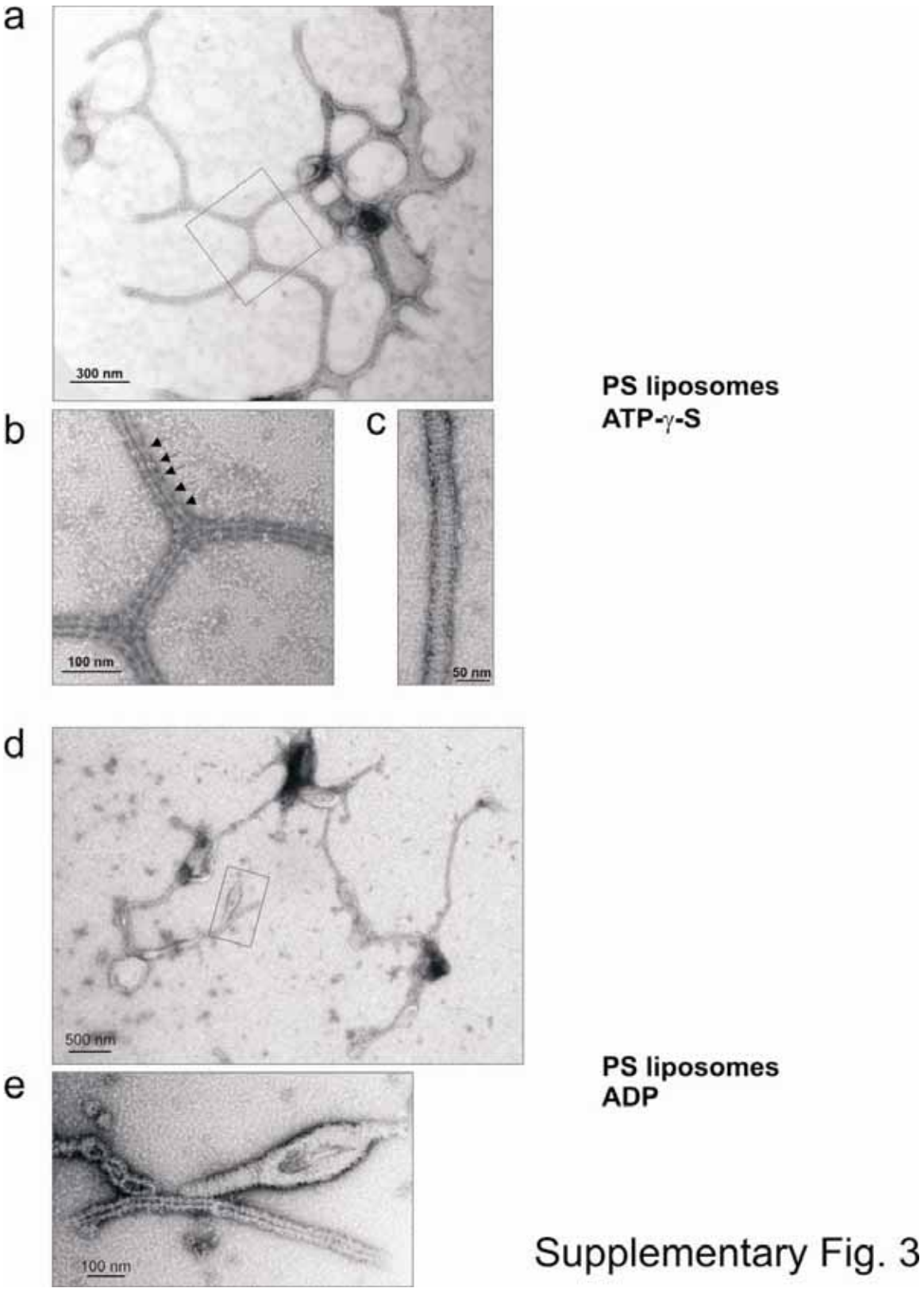

Supplementary Fig. 3

f

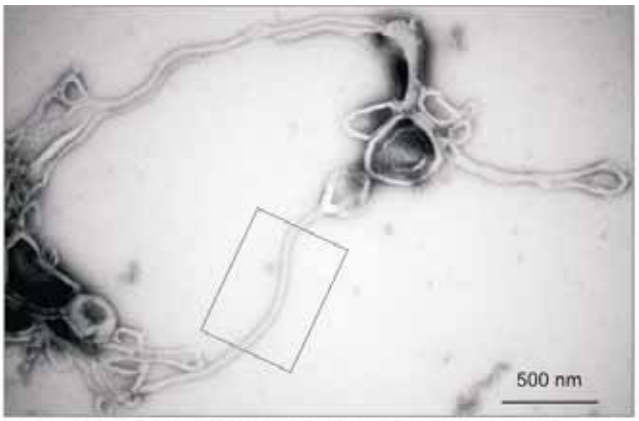

PS liposomes
no nucleotide

g

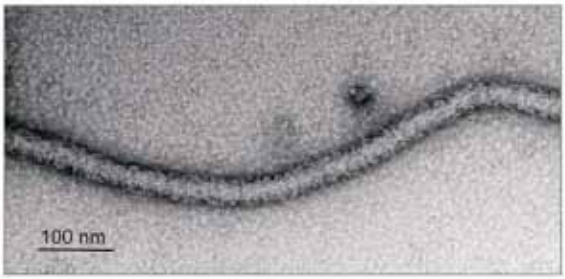

h

2.5% PIP_2
ATP-γ-S

i

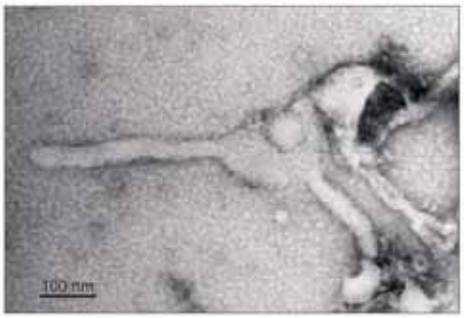

2.5% PIP_2
ADP

j

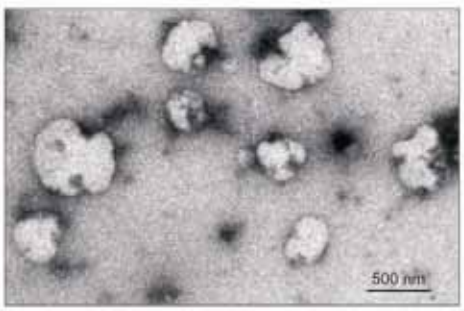

2.5% PIP_2
no nucleotide

Supplementary Fig. 3

Supplementary Figure 3: EHD2 tubulation of liposomes. EHD2 was incubated with the indicated liposomes in the presence and absence of nucleotides and analysed by EM as described in Methods. **a**, EHD2 deformed PS liposomes into tubular networks, here in the presence of ATP-γ-S. **b**, Enlarged views of the indicated area in a. Note the presence of regularly spaced EHD2 rings (some are indicated with arrows). This even spacing may be due to the curvature stress generated by an EHD2 ring along the axis of the lipid tubule which might disfavour binding of the next ring in the direct vicinity (see below). **c**, Some of the lipid tubules (especially at higher protein concentration) were tightly packed with EHD2 oligomeric rings. **d,e** In the presence of ADP and in the absence of nucleotide (**f,g**), EHD2 also tubulated PS liposomes and formed ring-like structures around the tubules. **e,g** are enlarged views of the indicated areas in d and f, respectively. We did not observe a noticeable change of size of the tubules with the different nucleotide conditions. **h,i,j**, Under less favourable lipid binding conditions (synthetic liposomes with 87.5% phosphatidyl-choline, 10% cholesterol and only 2.5% PIP_2), EHD2 tubulated liposomes in the presence of ATP-γ-S (h) and ADP (i), but we did not observe tubulation in the absence of nucleotides (j).

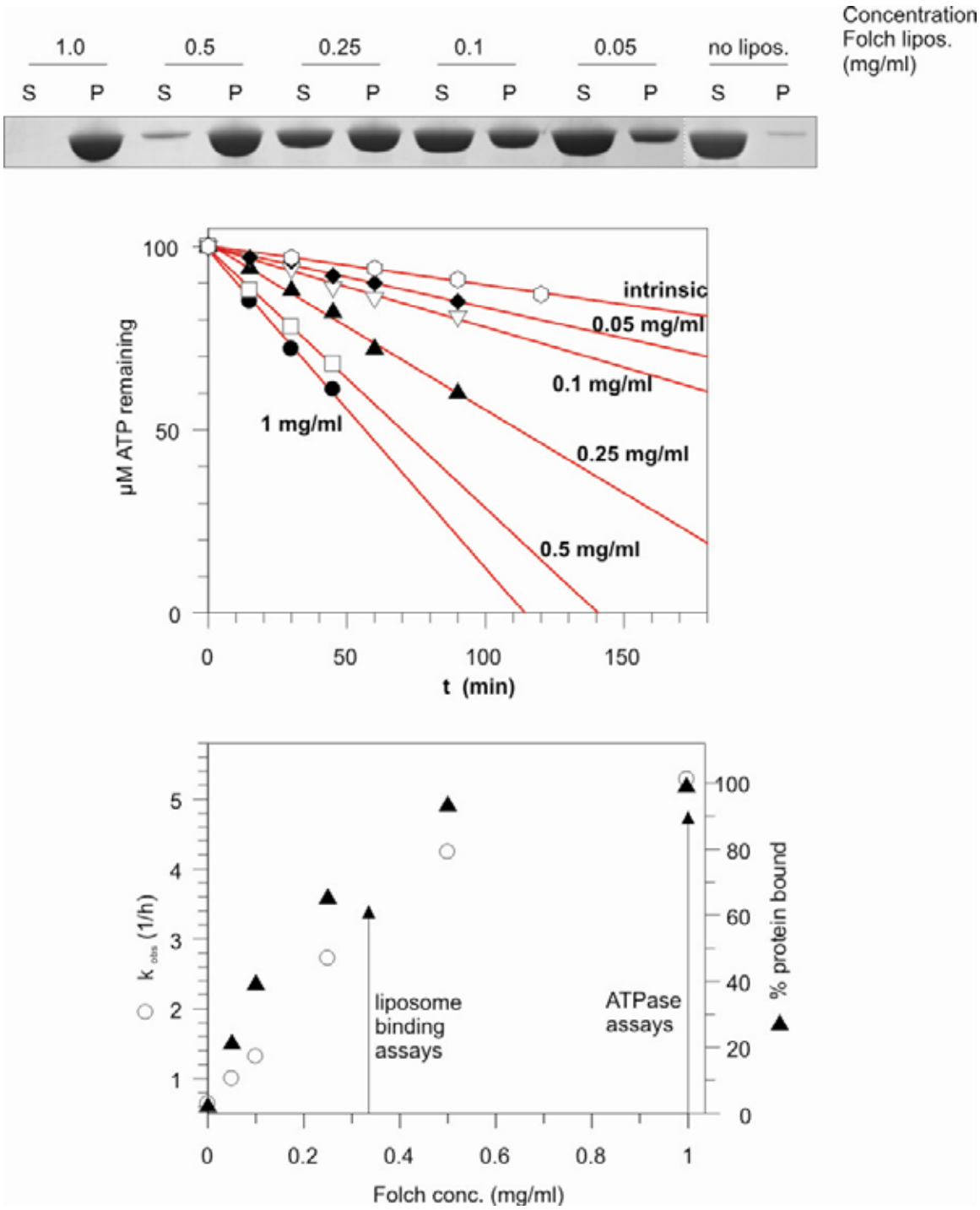

Supplementary Figure 4: a, Membrane binding of 10 μM EHD2 to 0.8 μm filtered Folch liposomes of the indicated concentration in the presence of 1 mM $MgCl_2$ and 1 mM ATP-γ-S. **b,** ATP hydrolysis, as measured by HPLC analysis, under the same conditions as in a. **c,** Observed rate and % liposome-bound EHD protein (measured by densitometry). The rate increased with increasing EHD2 bound to liposomes. In all further ATPase experiments 1 mg/ml Folch was used to determine the maximal rate. For liposome binding experiments we used 0.33 mg/ml Folch (unless otherwise indicated) to be in the range where binding differences could be better observed.

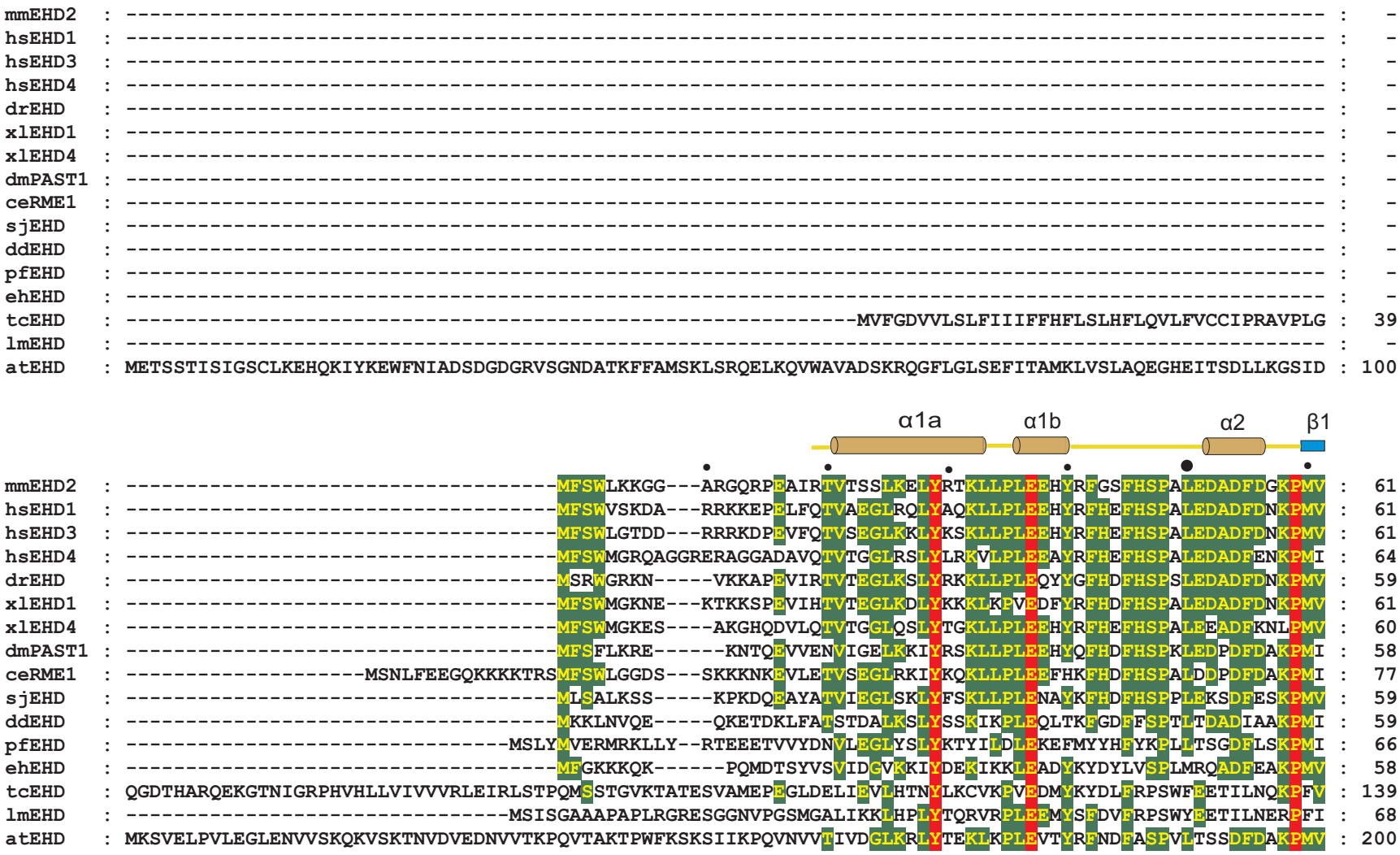

Supplementary Fig.5

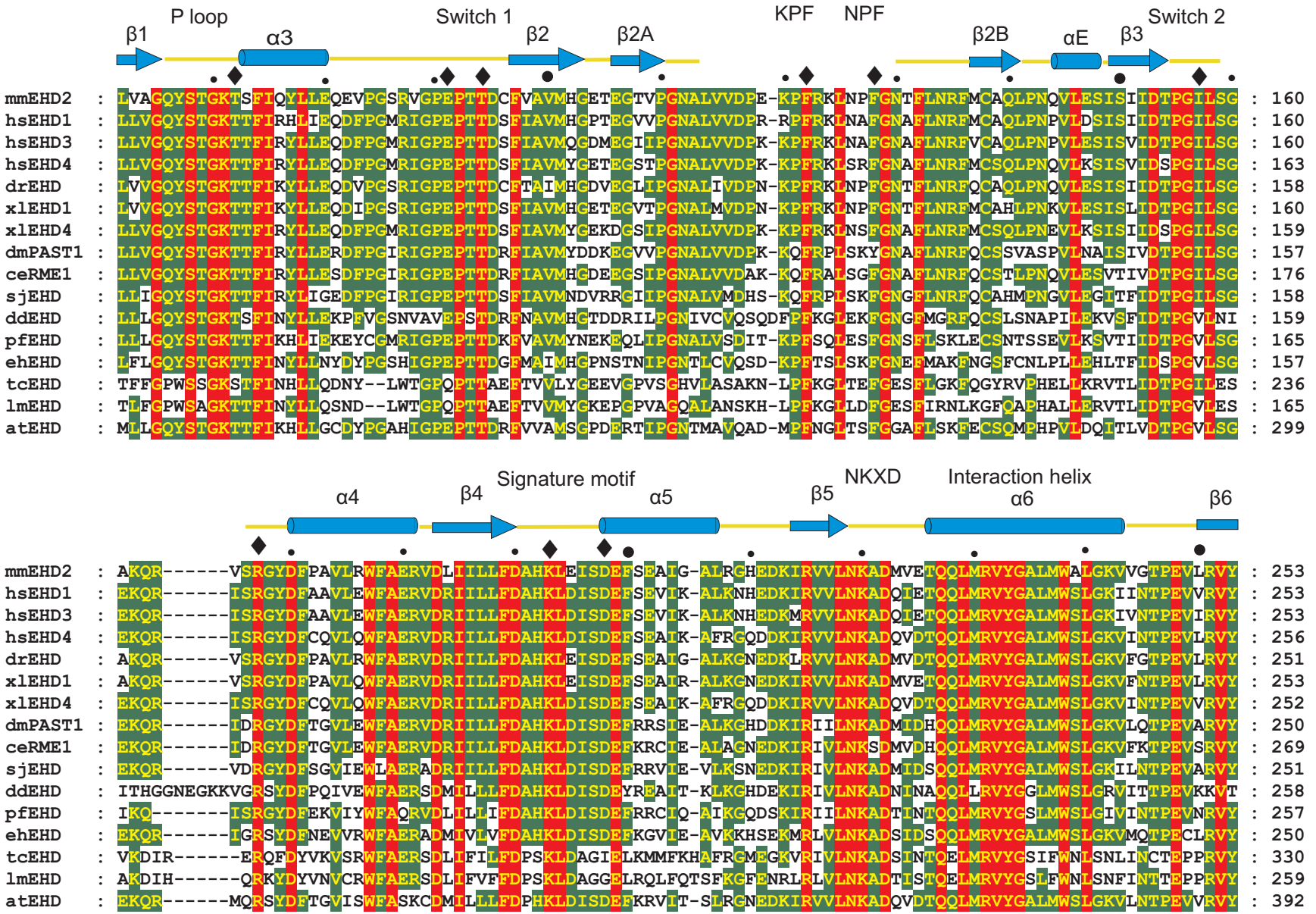

Supplementary Fig.5

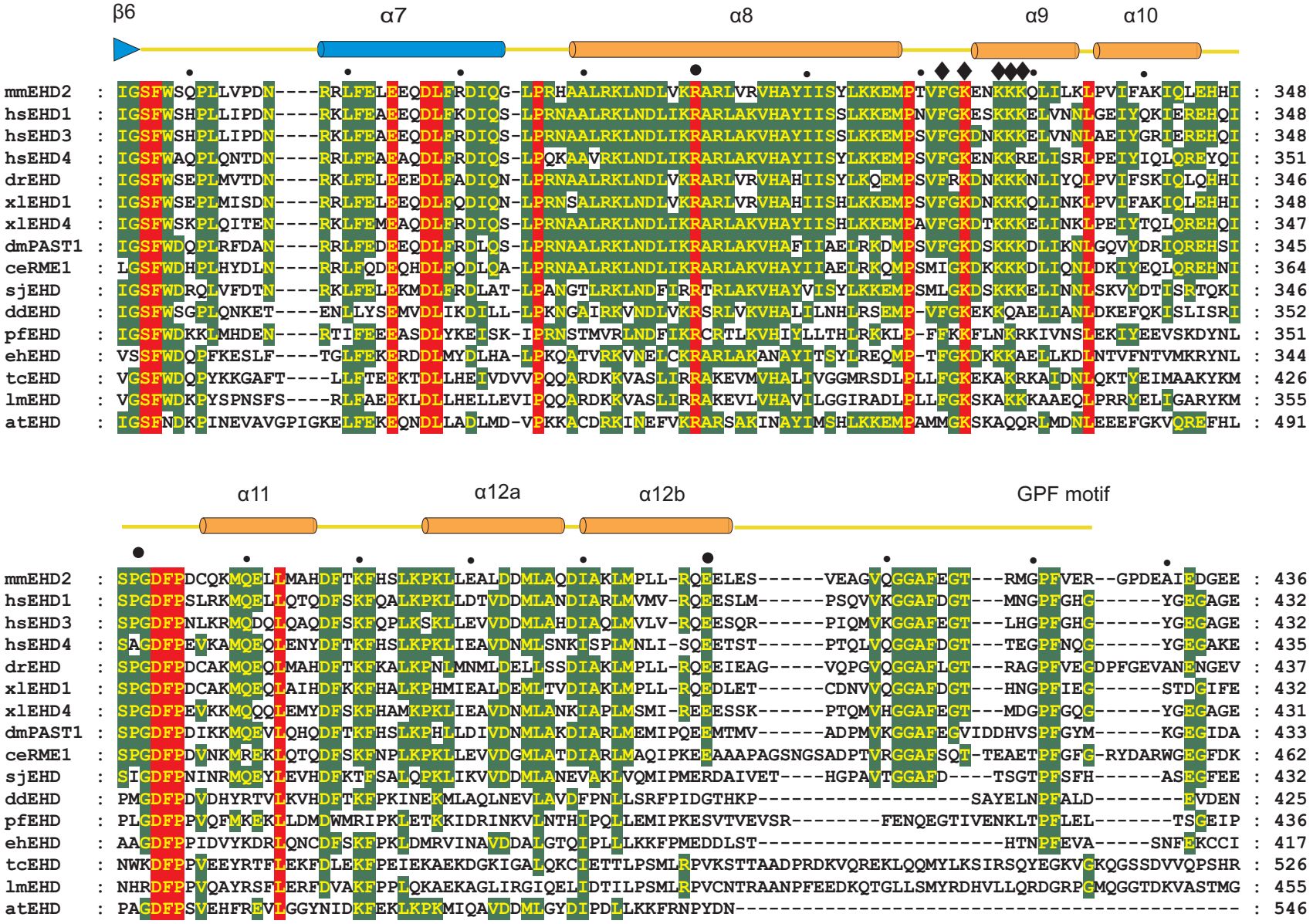

Supplementary Fig. 5

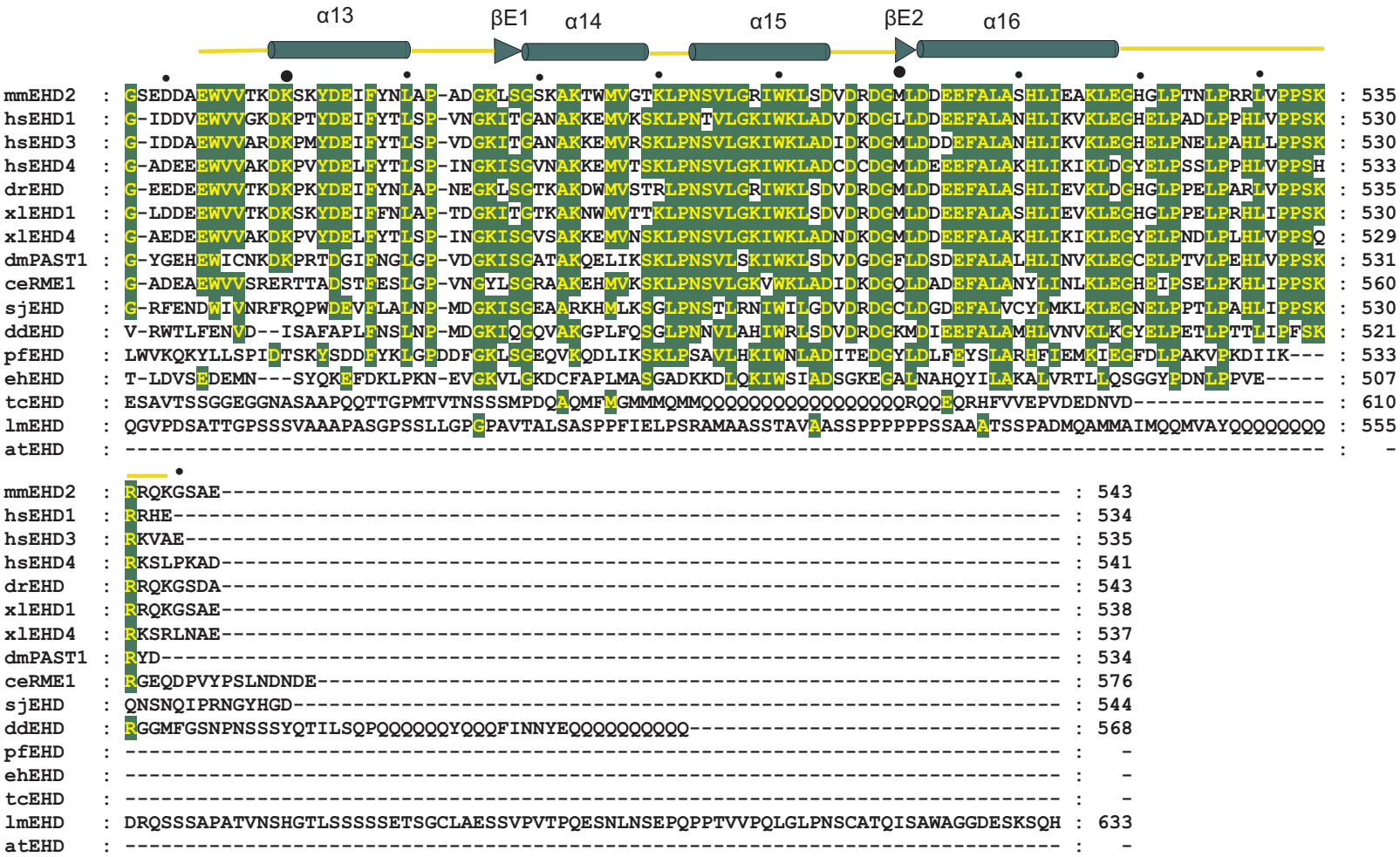

Supplementary Figure 5: Multiple sequence alignment of the EHD2 family and secondary structure assignment. The following sequences were aligned (expasy accession number in brackets): *Mus musculus* EHD2 (Q8BH64), *Homo sapiens* EHD1 (Q9H4M9), *Homo sapiens* EHD3 (Q9NZN3), *Homo sapiens* EHD4 (Q9H223), *Danio rerio* EHD (Q6P3J7), *Xenopus laevis* EHD1 (Q7SYA1), *Xenopus laevis* EHD4 (Q7ZXE8), *Drosophila melanogaster* PAST-1 (Q8IGN0), *Caenorhabditis elegans* RME1 (Q966F0), *Schistosoma japonicum* EHD (Q5DG45), *Dictyostelium discoideum* EHD (Q54ST5), *Plasmodium falciparum* EHD (Q9NLB8), *Entamoeba histolytica* EHD (Q515L4), *Trypanosoma cruzi* EHD (Q4DYK9), *Leishmania major* EHD (Q4QDJ3S), *Arabidopsis thaliana* EHD (Q3EAA4). Completely conserved residues are boxed in red, conserved residues (> 50% sequence identity) are boxed in green. Helices are indicated as cylinders, β-strands as blue arrows with colours according to the domain organisation (see Fig. 1a). Residues mutated in this study are indicated with a diamond (♦).

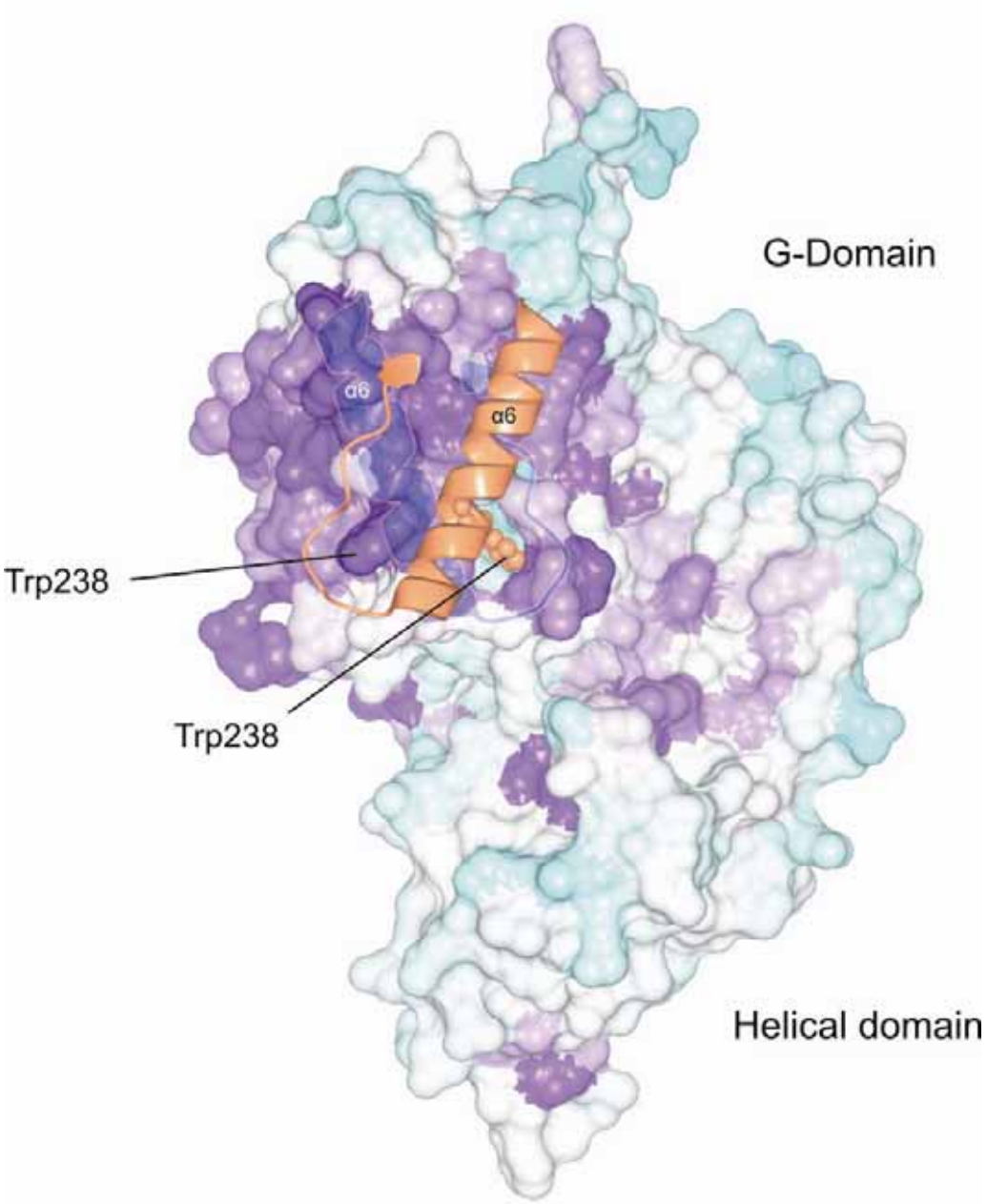

Supplementary Figure 6: The EHD dimer interface. The alignment in Supplementary Fig. 5 was used to create a surface conservation plot of the EHD2 G-domain and helical domain, with conserved residues shown in purple and non-conserved residues shown in cyan. Helix α6 with its invariant W238 and the contiguous loop of the opposing EHD2 monomer are shown in orange interacting with the conserved surface.

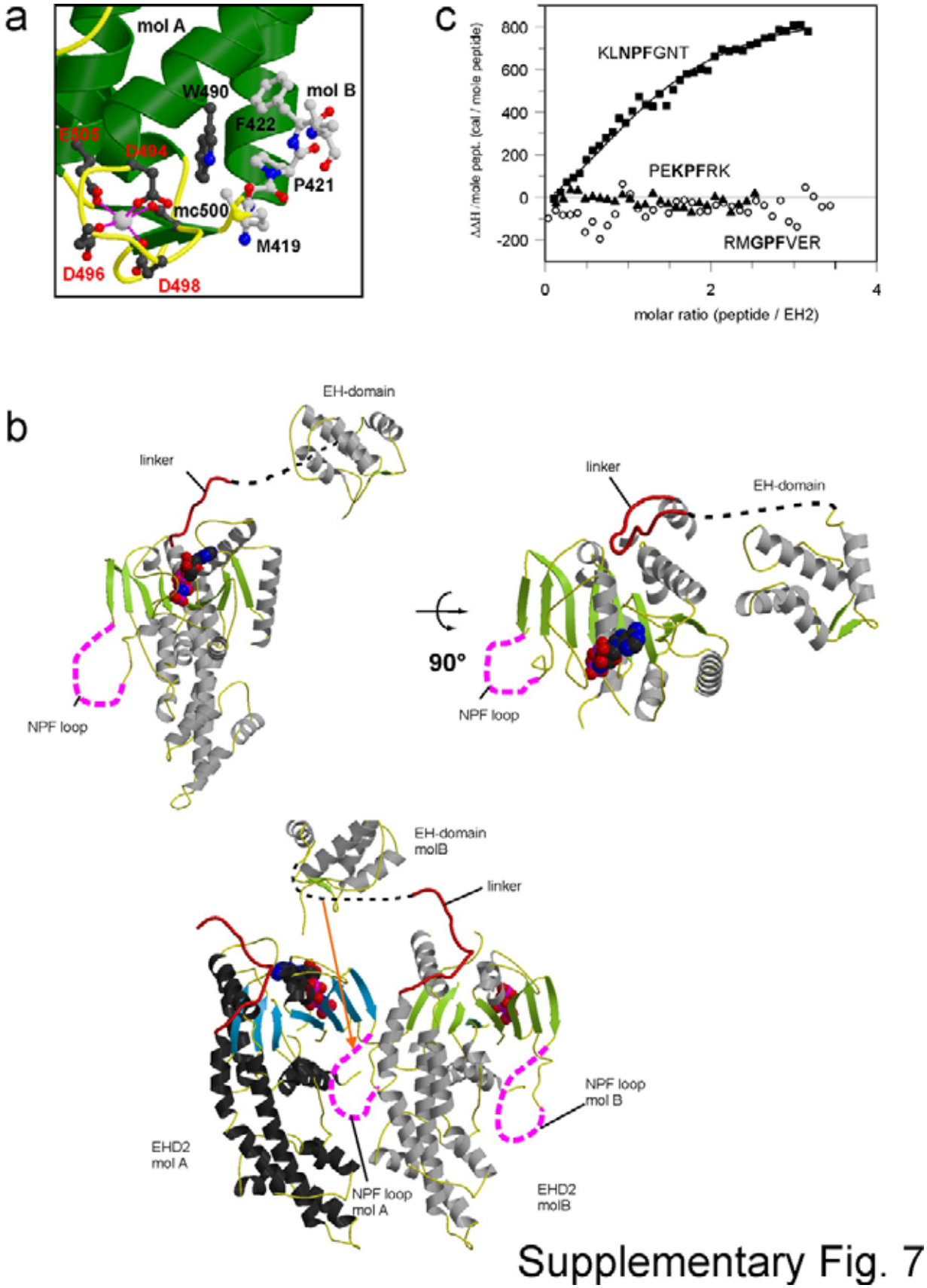

Supplementary Fig. 7

Supplementary Figure 7: EH-domain interactions. **a,** The Ca^{2+}-binding site of the EH-domain. Residues involved in Ca^{2+}-binding and W490 at the bottom of the peptide binding pocket are in dark grey and the bound GPF-peptide from the opposing molecule is in light grey. Five direct ligands for the Ca^{2+}-ion which has been maintained during purification could be identified which are the carboxy side-chains of D494, D496, D498, E505 and one main chain oxygen from M500 (mc500). The sixth ligands might be a water molecule not seen at the current resolution. **b**, Top and side view of the EHD2 monomer with the EH-domain linker shown in red and the NPF containing loop in magenta. Since the EH-domain linker is on the opposite face of the G-domain to the NPF containing loop, we argue that binding of the EH-domain to the NPF motif of the same molecule is sterically restricted. On the bottom, two adjacent monomers from the predicted EHD2 oligomer are shown (compare Fig. 4c). In this case, the EH-domain could bind without steric hindrance to the NPF containing loop of the adjacent monomer. **c,** Analysis of peptide binding to the EH-domain. The affinity of hepta-peptides from EHD2 containing the indicated xPF motifs to the EH-domain of EHD2 was measured by ITC at 10 °C in 100 mM HEPES (pH 7.5), 50 mM NaCl, 200 µM $CaCl_2$. Peptides ^{118}PEKPFRKL and ^{418}RMGPFVER did not show detectable binding whereas binding of peptide ^{124}KLNPFGNT could be fitted to an affinity of 130 $\pm$ 20 µM (n=1.33). This affinity is well within the range of other related EH-domain interactions[18]. The weak interaction between the GPF motif and the EH-domain and the C-terminal tail with R536 anchored in the nucleotide binding site could well prevent EHD2 from self-assembling in solution since the local concentration of the EH-domain in the dimer is high. Upon concentration of EHD2 at the lipid surface, however, a switch of the EH-domain to the high affinity side-site NPF motif of the adjacent dimer might be favoured. Furthermore, the EH-domain might be displaced from the top site during oligomerisation since its C-terminal tail with R536 is pointing into the predicted G-domain oligomerisation interface and would clash upon oligomerisation. The presence of two (or more) low-affinity interaction sites during protein complex assembly on membranes is a common theme also in clathrin-mediated endocytosis - it guarantees stable complex formation with a high degree of reversibility[41]. Our data do not exclude the possibility that EHDs are initially recruited to sites of action by NPF motif containing binding partners. However, we did not observe any co-localisation of described EHD binding partners, pacsin1 and 2 (ref. 12) along the length of EHD tubules *in vivo* (data not shown). The importance of a flexible linker between the helical and the EH-domains is underpinned by a dominant negative mutant in *C. elegans* Rme1 which is a point mutant of this linker[3].

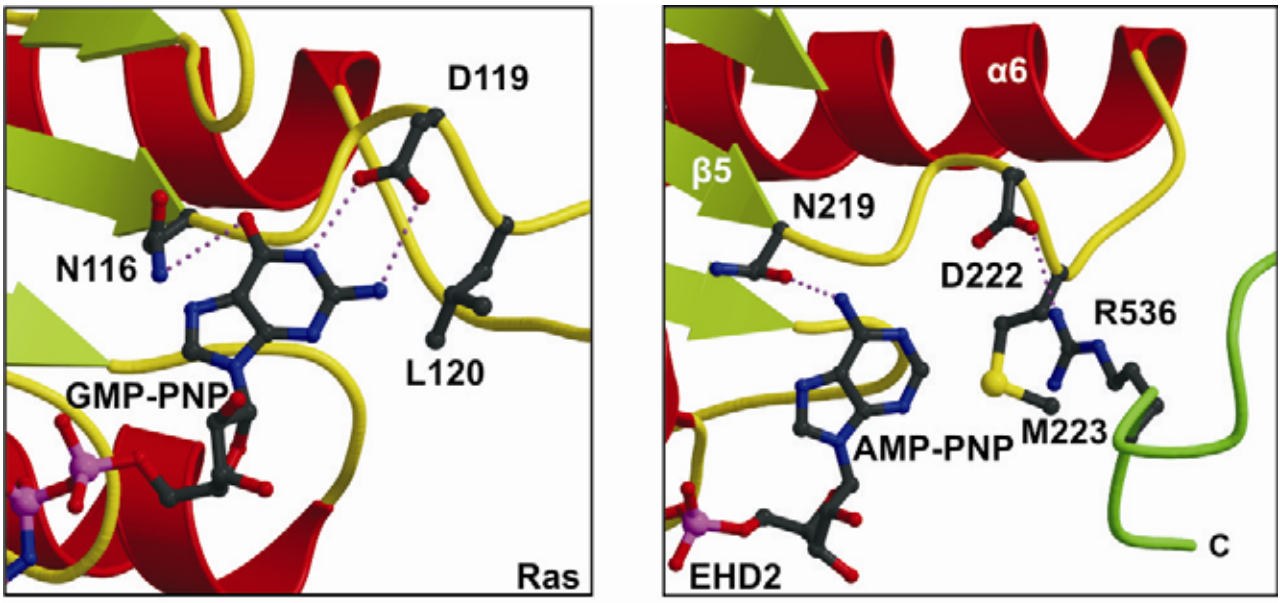

Supplementary Figure 8: Comparison of the nucleotide-binding sites of Ras (pdb code 5p21, left) and EHD2 (right). Residues from the NKxD motif involved in specific nucleotide recognition are shown with hydrogen bonds indicated. Specific guanosine recognition in GTPases is mediated by a highly conserved NKxD motif (called G4) where the asparagine side-chain forms a hydrogen bond to the carbonyl group at carbon6 of the guanosine base and the aspartate side-chain forms a double hydrogen bond to nitrogen1 of the guanosine base and the amine group at carbon2 (left). Aspartate has been shown to be crucial since mutating it to asparagine in Ras reduces nucleotide affinity by more than 1000-fold[42]. Directly following the NKxD motif, a large hydrophobic residue (leucine in Ras and dynamin, M223 in EHD2) lines the nucleotide binding pocket. The NKxD motif of EHD2 (starting at residue 219) is also highly conserved in EHD family members (Supplementary Fig. 5). The carboxyamide group of N219 forms a hydrogen bond to the C6 amino group of the adenine base (right). M223, whose side-chain is buttressed by the side chain of H192 (not shown), is closer to the purine base than the corresponding leucine residue in Ras and sterically excludes accommodation of an amino group at C2, thus explaining the inability of EHDs to bind to guanine nucleotides. Instead of forming a double hydrogen bond, the completely invariant D222 of EHD2 surprisingly forms a salt bridge with the conserved R536 which is supplied from the C-terminus of the superjacent EH-domain (right). This arginine is not contributing to nucleotide binding since the EHD without the EH-domain binds with the same affinity to ATP-γ-S (data not shown).

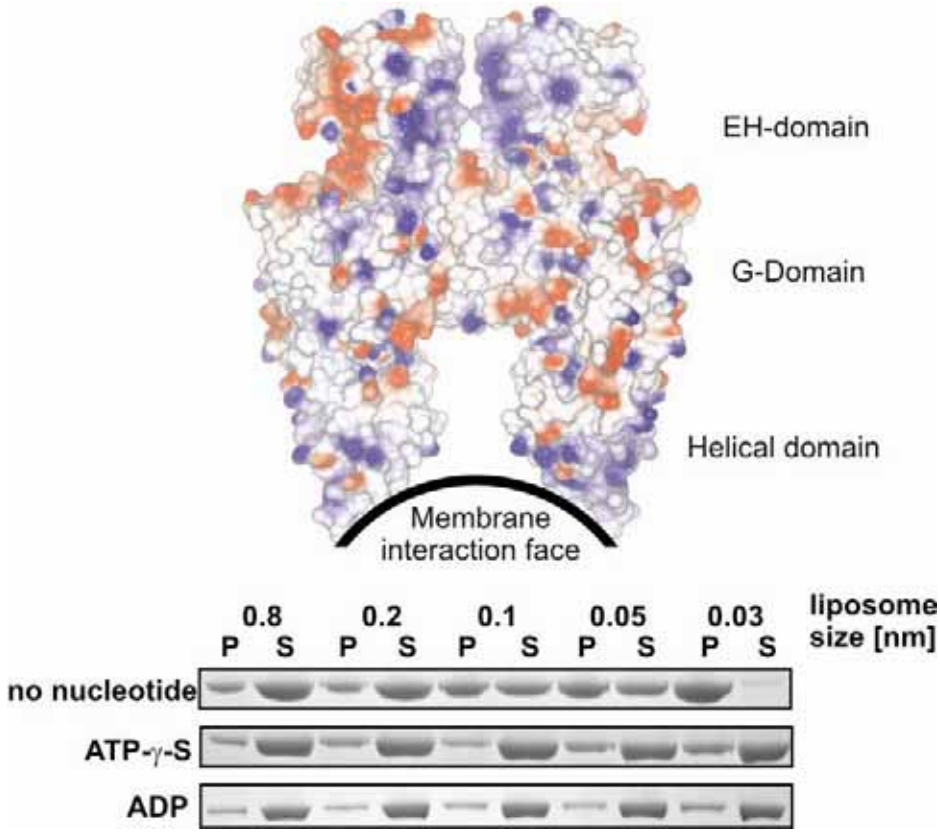

Supplementary Figure 9: Top: Electrostatic surface representation of EHD2. Red indicates negative charge and blue positive charge at neutral pH. The orientation of EHD2 is the same as in Fig. 2a. The membrane interaction site is highly curved which is a consequence of EHD2 dimerisation. The diameter of the sphere is approximately 7 nm, but this may not be so extreme if the tips of the loops (a phenylalanine and a valine residue) are inserted into the membrane and if the membrane-binding sites show some flexibility. Bottom: EHD binding to liposomes of different sizes in the presence and absence of 1 mM nucleotides and 1 mM $MgCl_2$ (P - pelleted fraction, S -supernatant). We used synthetic liposomes containing 87.5% phosphatidyl-choline, 10% cholesterol and 2.5% PIP_2 at the same protein/lipid ratio as in Supplementary Fig. 3. The protein:membrane interaction is more stringent (lower affinity interaction) to these liposomes than to Folch or PS liposomes, and this allows us to look for nucleotide and liposome size dependency (curvature preference) of the interaction. We argue that a protein with a curved dimer interface, like that in the EHD2 dimer, should show curvature preference for small liposomes which have a curvature closely matching the curvature of the membrane-binding interface of the EHD2 dimer. As a result, no or less energy is required to deform the lipid bilayer of small liposomes to the preferred curvature. Preferred binding to small liposomes is precisely what we observed but only in the nucleotide-free state. In the nucleotide-bound state, we previously observed limited oligomerisation of the residual EHD2 protein bound to these liposomes by electron microscopy (Supplementary Fig. 3). In our predicted EHD2 oligomer (see Supplementary Fig. 12), there are two curvatures, the one formed by the lipid-binding interface of the dimer and the other formed by the oligomer. These are orthogonal to each other. Thus, while the EHD2 *dimer* in the ATP-bound state may still be expected to bind with higher affinity to small liposomes, we observe that the EHD2 *oligomer* makes tubules and energy is required for this lipid bilayer deformation. An oligomer bound to a vesicle of non-ideal curvature will have an increased off-rate, and thus we observed less binding in our experiments. The issue of curvature sensing versus curvature driving of membrane interacting proteins has been previously discussed[43].

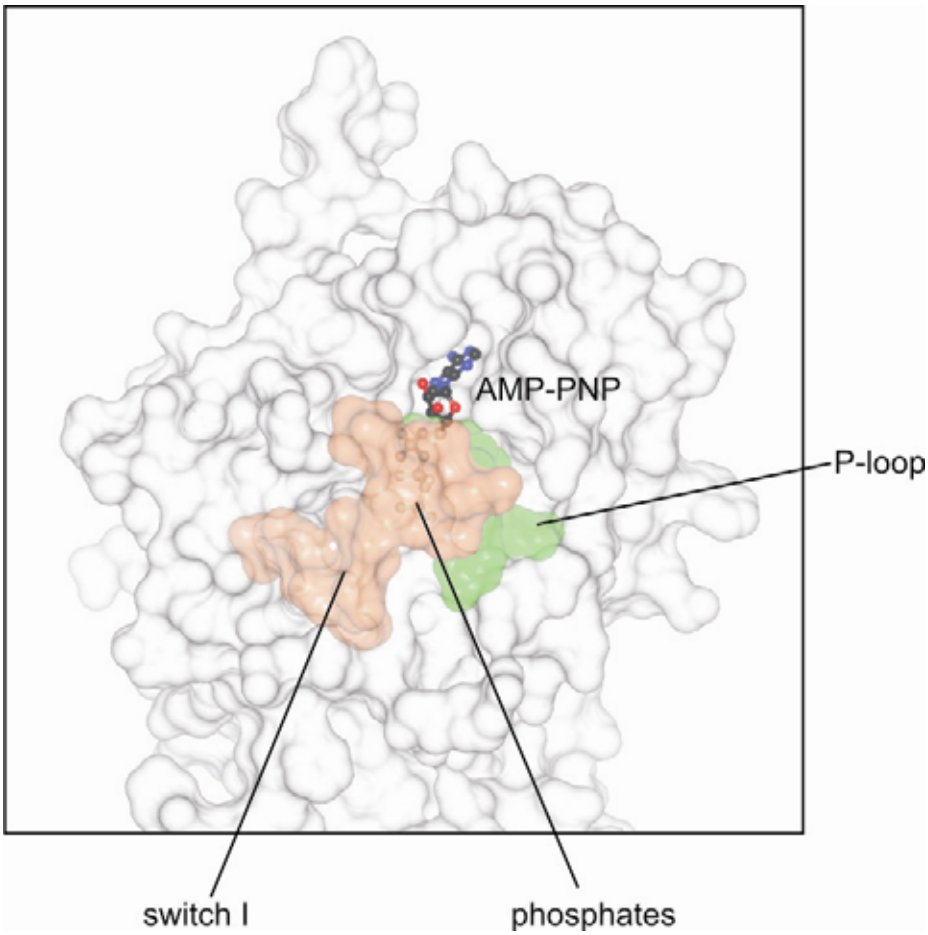

Supplementary Figure 10: Phosphate cap. The phosphates of the AMP-PNP molecule are covered by residues from switch I and the P-loop. This cap does not allow the insertion of a catalytic residue *in trans* into the active site. This so-called "phosphate cap" is also present in GBP1 (ref. 44) whose mechanism of GTP hydrolysis has been shown to involve dimerisation-dependent positioning of the attacking nucleophilic water molecule by a catalytic serine *in cis* from switch I (ref. 15).

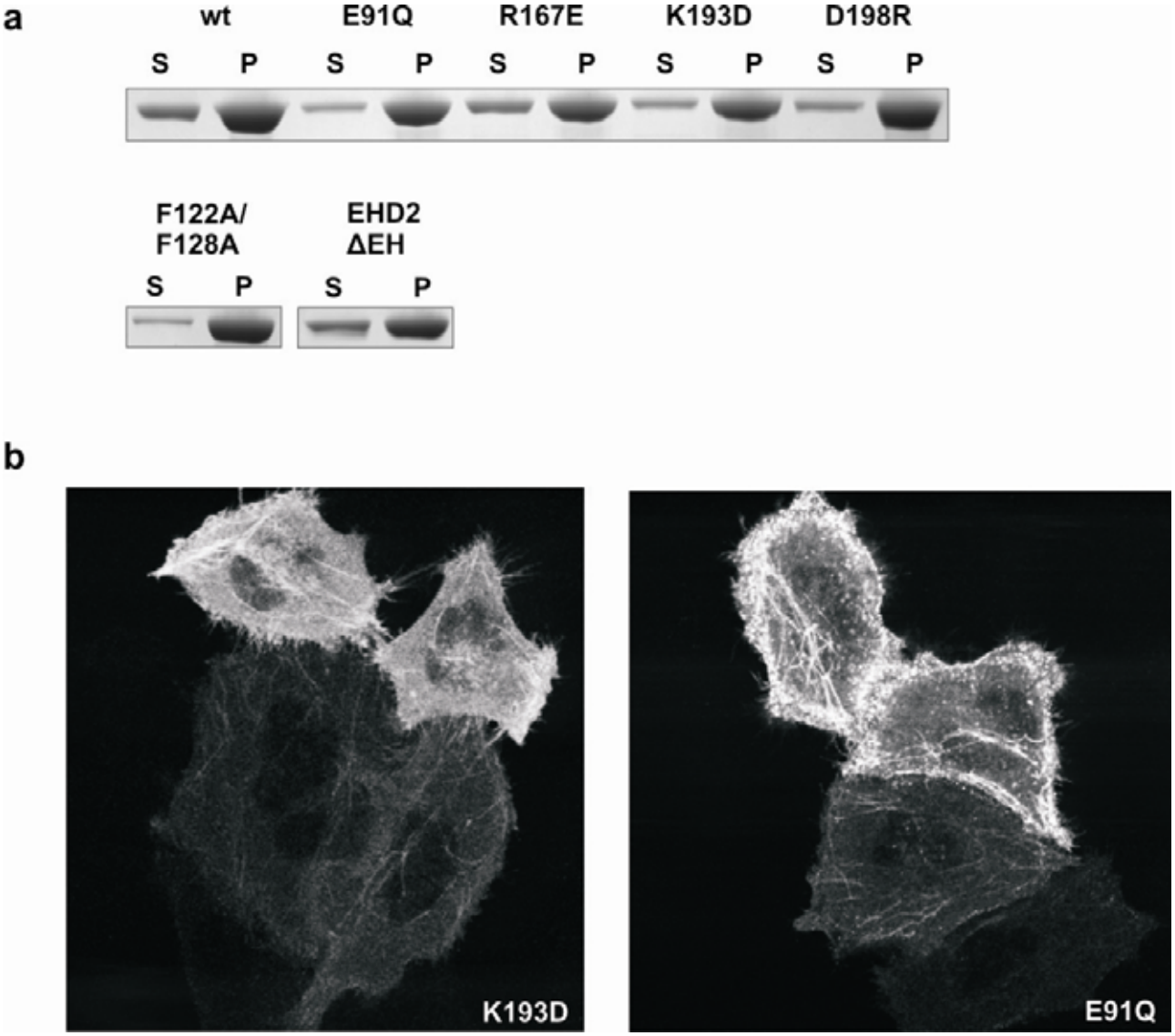

Supplementary Figure 11: a, Membrane binding of oligomerisation-interface mutants to Folch liposomes (methods as in Fig. 1c). **b,** The K193D mutant, which *in vitro* does not display any liposome-stimulated ATPase reaction, showed extensive tubulation with essentially no punctuate staining when over-expressed as EGFP-tagged protein in HeLa cells (100% cells showed a tubular phenotype, n=53). On the contrary, overexpression of the E91Q mutant, which *in vitro* had only a mildly impaired stimulated ATPase reaction, resulted in a similar phenotype as wild type EHD2, with 82% of the examined low-level expressing cells showing a tubular and punctuate phenotype, 16% showing only punctuate staining and 2% a tubular phenotype (n=43).

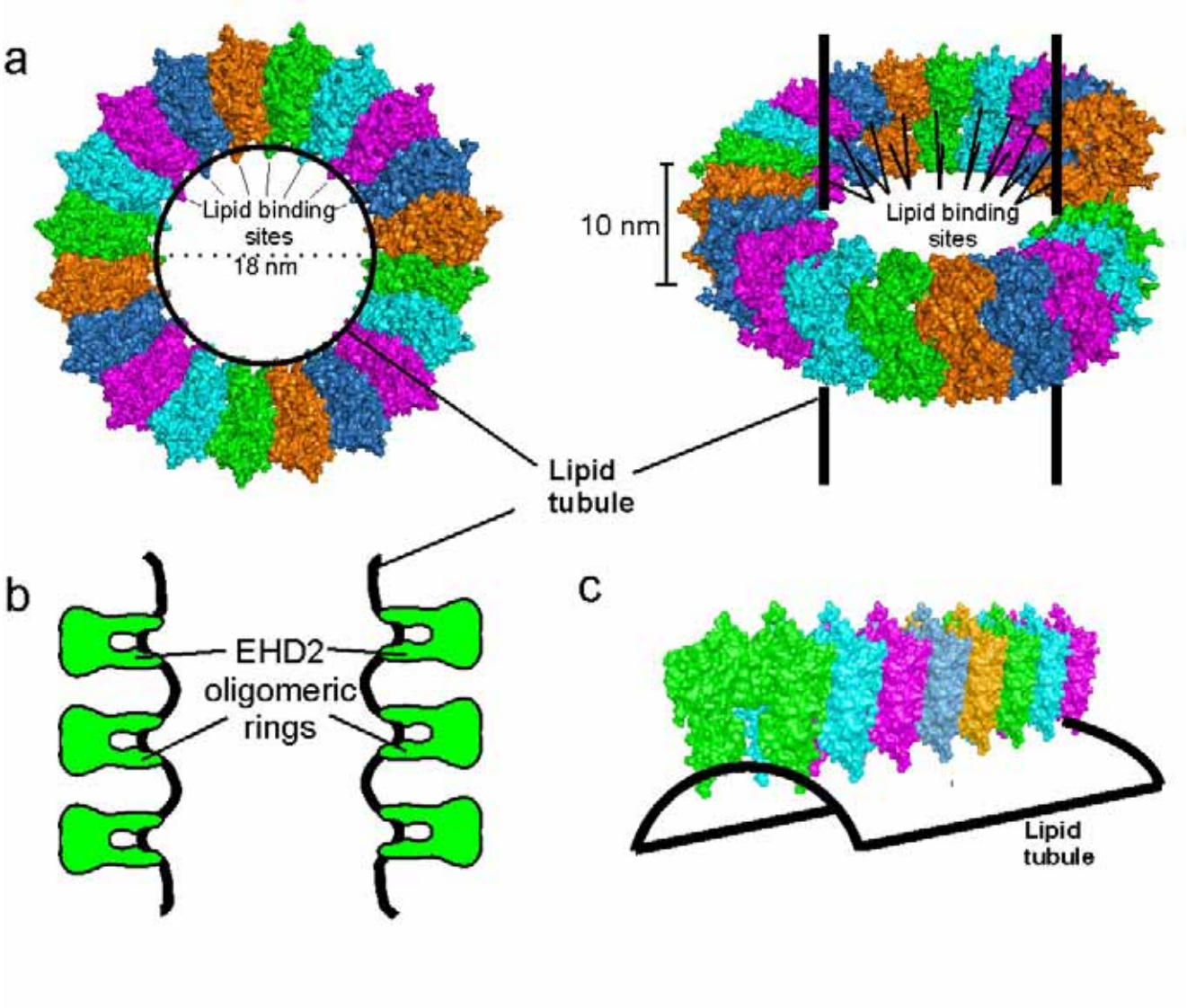

Supplementary Figure 12: a, Top and side view of the EHD2 oligomeric ring model in a surface representation. For better clarity, the EH-domains are not included. The diameter of the embraced lipid tubule is ≈18 nm and the thickness of the EHD2 ring is ≈10 nm, in agreement to what is observed in the EM assays. Approximately twenty EHD2 dimers constitute one turn in this model. **b**, Arrangement of the EHD2 dimers in the oligomer. The high curvature of the membrane interaction site of EHD2 (Supplementary Fig. 9) is oriented perpendicular to the curvature of the lipid tubule. This arrangement is predicted to induce local curvature on the lipid tubule. **c**, In an alternative model, the oligomer could also form along the length of a tubule (parallel to its long axis) and thus maximise the use of the highly curved membrane interface of the dimer. However, such an arrangement was never observed by EM (Fig. 1d, Supplementary Fig. 3). Furthermore, our ring-based oligomer model is consistent with the absence of any curvature-sensitive membrane binding upon oligomerisation.

Supplementary Table 1 Data collection statistics

	Selenomethionine derivative
Data collection	
Space group	C2
Cell dimensions	
a, *b*, *c* (Å)	99.9, 134.7, 56.1
α, β, γ (º)	90, 106.5, 90
Wavelength	0.97962
Resolution (Å) *	20 – 3.1 (3.2 – 3.1)
R_{sym} *	7.8 (36.1)
$I/\sigma I$ *	11.45 (4.4)
Completeness (%)*	96.4 (93.8)
Redundancy *	3.4 (3.4)

*Highest resolution shell is shown in parenthesis.

Supplementary notes / Supplementary References

23. Lenzen, C., Cool, R. H. & Wittinghofer, A. Analysis of intrinsic and CDC25-stimulated guanine nucleotide exchange of p21ras-nucleotide complexes by fluorescence measurements. *Methods Enzymol.* **255**, 95-109 (1995).
24. Van Duyne, G. D., Standaert, R. F., Karplus, P. A., Schreiber, S. L. & Clardy, J. Atomic structures of the human immunophilin FKBP-12 complexes with FK506 and rapamycin. *J. Mol. Biol.* **229**, 105-124 (1993).
25. Kabsch, W. Automatic Processing of Rotation Diffraction Data from Crystals of Initially Unknown Symmetry and Cell Constants. *Journal of Applied Crystallography* **26**, 795-800 (1993).
26. Sheldrick, G. M. & Schneider, T. R. in *Macromolecular Crystallography, Pt B* 319-343 (1997).
27. de la Fortelle, E. & Bricogne, G. in *Methods in Enzymology* (eds. Carter, C. W., Jr & Sweet, R. M.) 472-494 (1997).
28. McRee, D. E. XtalView/Xfit--A versatile program for manipulating atomic coordinates and electron density. *J Struct Biol* **125**, 156-65 (1999).
29. Murshudov, G. N., Vagin, A. A. & Dodson, E. J. Refinement of Macromolecular Structures by the Maximum-Likelihood Method. *Acta Cryst.* **D53**, 240 (1997).
30. Laskowski, R. A., Macarthur, M. W., Moss, D. S. & Thornton, J. M. Procheck - a Program to Check the Stereochemical Quality of Protein Structures. *Journal of Applied Crystallography* **26**, 283-291 (1993).
31. Kraulis, P. J. Molscript - a Program to Produce Both Detailed and Schematic Plots of Protein Structures. *Journal of Applied Crystallography* **24**, 946-950 (1991).
32. Merritt, E. A. & Murphy, M. E. Raster3D Version 2.0. A program for photorealistic molecular graphics. *Acta Crystallogr D Biol Crystallogr* **50**, 869-73 (1994).
33. Landau, M. et al. ConSurf 2005: the projection of evolutionary conservation scores of residues on protein structures. *Nucleic Acids Research* **33**, W299-W302 (2005).
34. Potterton, E., McNicholas, S., Krissinel, E., Cowtan, K. & Noble, M. The CCP4 molecular-graphics project. *Acta Crystallographica Section D-Biological Crystallography* **58**, 1955-1957 (2002).
35. DeLano, W. L. *The PyMOL Molecular Graphics System* (DeLano Scientific, Palo Alto, CA, USA, 2002).
36. Guex, N. & Peitsch, M. C. SWISS-MODEL and the Swiss-PdbViewer: An environment for comparative protein modeling. *Electrophoresis* **18**, 2714-2723 (1997).
37. Collaborative Computational Project, N. The CCP4 suite: programs for protein crystallography. *Acta Crystallogr. D* **50**, 760 (1994).
38. Philo, J. S. A method for directly fitting the time derivative of sedimentation velocity data and an alternative algorithm for calculating sedimentation coefficient distribution functions. *Analyt. Biochem.* **279**, 151-163 (2000).
39. Philo, J. S. Improved methods for fitting sedimentation coefficient distributions derived by time-derivative techniques. *Analyt. Biochem.* **354**, 238-246 (2006).
40. Laue, T. M., Shah, B. D., Ridgeway, T. M. & Pelletier, S. L. in *Analytical Ultracentrifugation in Biochemistry and Polymer Science* (eds. Harding, S. E., Rowe, A. J. & Horton, J. C.) 90-125 (Royal Society of Chemistry, Cambridge, UK, 1992).
41. Schmid, E. M. et al. Role of the AP2 beta-appendage hub in recruiting partners for CCV assembly. *PLoS Biol.* **4**, e262 (2006).

42. Schmidt, G. et al. Biochemical and biological consequences of changing the specificity of p21ras from guanosine to xanthosine nucleotides. *Oncogene* **12**, 87-96 (1996).
43. McMahon, H. T. & Gallop, J. L. Membrane curvature and mechanisms of dynamic cell membrane remodelling. *Nature* **438**, 590-6 (2005).
44. Prakash, B., Renault, L., Praefcke, G. J., Herrmann, C. & Wittinghofer, A. Triphosphate structure of guanylate-binding protein 1 and implications for nucleotide binding and GTPase mechanism. *EMBO J.* **19**, 4555-4564 (2000).